THE GEOLOGICAL SOCIETY OF AMERICA®

Isotopic signatures of mercury contamination in latest Permian oceans

Stephen E. Grasby[1,2*], Wenjie Shen[3], Runsheng Yin[4,5], James D. Gleason[6], Joel D. Blum[6], Ryan F. Lepak[5], James P. Hurley[5], and Benoit Beauchamp[2]

[1]Geological Survey of Canada, Natural Resources Canada, 3303 33rd Street N.W., Calgary, Alberta T2L 2A7, Canada
[2]Department of Geoscience, University of Calgary, 2500 University Drive N.W., Alberta T2N 1N4, Canada
[3]School of Earth Science and Geological Engineering, Sun Yat-sen University, Guangzhou 510275, China
[4]State Key Laboratory of Ore Deposit Geochemistry, Institute of Geochemistry, Chinese Academy of Sciences, Guiyang 550002, China
[5]Environmental Chemistry and Technology Program, University of Wisconsin–Madison, Madison, Wisconsin 53706, USA
[6]Department of Earth and Environmental Sciences, University of Michigan, Ann Arbor, Michigan 48109, USA

ABSTRACT

Sedimentary records from the northwest margin of Pangea and the Tethys show anomalously high Hg levels at the latest Permian extinction boundary. Background δ^{202}Hg values are consistent with normal marine conditions but exhibit negative shifts coincident with increased Hg concentrations. Hg isotope mass-independent fractionation (Δ^{199}Hg) trends are consistent with volcanic input in deep-water marine environments. In contrast, nearshore environments have Δ^{199}Hg signatures consistent with enhanced soil and/or biomass input. We hypothesize that the deep-water signature represents an overall global increase in volcanic Hg input and that this isotope signature is overwhelmed in nearshore locations due to Hg from terrestrial sources. High-productivity nearshore regions may have experienced stressed marine ecosystems due to enhanced Hg loading.

INTRODUCTION

An anomalous spike in Hg concentrations observed at the latest Permian extinction (LPE) boundary is thought to be associated with contemporaneous Siberian Trap eruptions (Grasby et al., 2015a; Sanei et al., 2012). Hg spikes have subsequently been recognized at several other mass extinction boundaries associated with large igneous province (LIP) events (Grasby et al., 2015b; Percival et al., 2015; Sial et al., 2013; Thibodeau et al., 2016). It remains unclear, however, if volcanic eruptions were the sole source of anomalous Hg deposition, or if other Hg sources and pathways related to environmental perturbations by LIPs were also significant. This is critical for tracing Hg fluxes to the environment during mass extinctions, as a marker of volcanism, as well as elucidating potential deleterious impacts on global ecosystems. We examined mercury stable isotopes across the LPE because they display both mass-dependent fractionation (MDF, reported as δ^{202}Hg) and mass-independent fractionation of odd-mass-number isotopes (MIF, reported as Δ^{199}Hg) that yield important information on Hg sources and cycling (Blum et al., 2014).

BACKGROUND

The LPE was the most severe mass extinction in Earth history (Chen and Benton, 2012; Erwin et al., 2002). The LPE was closely linked with the Siberian Trap eruptions that occurred over 800 k.y., starting ~300 k.y. prior to the LPE (Burgess and Bowring, 2015). Along with impacts on marine ecosystems (Chen and Benton, 2012), the eruptions caused massive soil erosion (Algeo and Twitchett, 2010) related to denudation of terrestrial plant cover and wildfires (Benton and Newell, 2014). The exact causal connection between eruption and extinction processes is, however, uncertain. One significant impact would be toxic metal release. It is estimated that Hg emission rates from the Siberian Traps were 0.8–10 Gg/yr (Grasby et al., 2015a): 32%–399% above modern geogenic sources and comparable to the ~2.2 Gg/yr of anthropogenic Hg released at present (Pacyna and Pacyna, 2001).

METHODS

We examined the extinction boundary from two marine settings of Pangea (Fig. 1): (1) the Buchanan Lake section from the Sverdrup Basin, Canadian Arctic Archipelago (Grasby and Beauchamp, 2009), and (2) the Meishan section, China (Yin et al., 2001). Buchanan Lake records sedimentation from the mid-latitude boreal margin of northwest Pangea in a bathyal to near-abyssal environment (deep water far from shore), whereas Meishan represents an equatorial environment within the Tethys Sea (Fig. 1) in a clastic sediment–starved carbonate platform setting. The Meishan section is highly condensed relative to Buchanan Lake (Grasby and Beauchamp, 2009). For comparison, we used the datum for the LPE event boundary as correlated by Grasby and Beauchamp (2009).

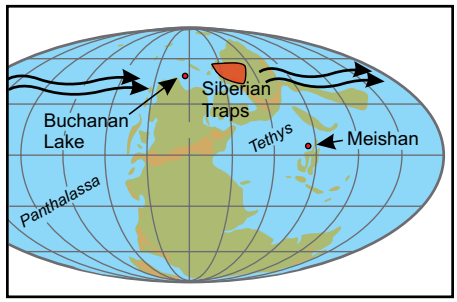

Figure 1. Paleogeographic map showing sections studied, in Late Permian time, relative to Siberian Traps and prevailing trade winds.

Due to the strong bonding of Hg to organic matter and reduced sulfur in sediments, Hg does not show significant fractionation during burial/heating of sedimentary rocks (Smith et al., 2008). Thus, variations of Hg isotopes in sedimentary rocks have been explained by source changes rather than diagenetic effects (Thibodeau et al., 2016). Hg isotopic composition is expressed in δ^{202}Hg notation referenced to the NIST-3133 Hg standard:

$$\delta^{202}\mathrm{Hg}\ (‰) = [(^{202}\mathrm{Hg}/^{198}\mathrm{Hg}_{\mathrm{sample}})/(^{202}\mathrm{Hg}/^{198}\mathrm{Hg}_{\mathrm{standard}}) - 1] \times 1000. \quad (1)$$

MIF is reported in Δ notation (Δ^{xxx}Hg), describing the difference between the measured δ^{xxx}Hg and the theoretically predicted δ^{xxx}Hg value:

$$^{xxx}\mathrm{Hg}\ (‰) \approx \delta^{xxx}\mathrm{Hg} - \delta^{202}\mathrm{Hg} \times \beta. \quad (2)$$

Detailed sampling and laboratory methods are given in the GSA Data Repository[1].

*E-mail: steve.grasby@canada.ca

[1]GSA Data Repository item 2017014, detailed sampling and laboratory methods, is available online at http://www.geosociety.org/pubs/ft2017.htm or on request from editing@geosociety.org.

RESULTS

The two sections show relatively constant background Hg concentrations, both absolute and when normalized by total organic carbon (TOC) to account for Hg drawdown by organic matter (Fig. 2; Grasby et al., 2013). At the LPE boundary, both sections shift to higher Hg concentrations and Hg/TOC. At Buchanan Lake, earlier spikes in Hg concentrations are related to coal ash deposition (Grasby et al., 2011); however, the main shift in Hg/TOC is at the LPE. Baseline δ^{202}Hg values (taken as the lowest position in the sections) are ~–0.39‰ at Buchanan Lake and –0.65‰ at Meishan. Both sections show a negative deviation in δ^{202}Hg just prior to the LPE, low values across the extinction, and then a return toward baseline values (Figs. 2B and 2E). Vertical lines in Figure 2 show our defined baseline and minimum values for Meishan to aid comparison.

A small but significant MIF signal was also observed. The overall average Δ^{199}Hg/Δ^{201}Hg value of 1.08 ± 0.27 (Fig. 3A) for both sections is consistent with values for photoreduction of aqueous Hg(II) driven by natural dissolved organic matter (average of 1.02; Bergquist and Blum, 2007). For pre-extinction samples, Δ^{199}Hg values of ~+0.15‰ were observed in Buchanan Lake and ~+0.10‰ at Meishan (Figs. 2C and 2F). At the LPE, Buchanan Lake showed a slight positive shift in Δ^{199}Hg values (from 0.12‰ to 0.18‰), whereas Meishan had a significant negative shift (to –0.12‰; Figs. 2C and 2F).

DISCUSSION

Mercury spikes at the LPE boundary in both sections are coincident with abundant framboidal pyrite rainout related to a switch to euxinic ocean conditions (Grasby and Beauchamp, 2009; Shen et al., 2007). A coincident shift to higher Hg/TOC reflects enhanced Hg loading and sulfide scavenging (Sanei et al., 2012). Thus, Hg loading to the marine environment appears to have been a global event. Stable isotopes of Hg provide insight into the sources and pathways of this Hg (Fig. 4).

Background Hg Source

Background δ^{202}Hg values of ~–0.50‰ are consistent with that reported for pre-anthropogenic marine sediments (δ^{202}Hg of –0.76‰ ± 0.16‰; Gehrke et al., 2009), and the relatively narrow δ^{202}Hg values (~–0.60‰) of most geogenic sources (Sherman et al., 2009; Smith et al., 2008; Yin et al., 2016). While Hg released into the environment can undergo complicated geochemical transformation processes resulting in large variations of δ^{202}Hg (>10‰), transport and burial result in mixing and homogenization of Hg, such that marine δ^{202}Hg has a narrow range reflecting the original geogenic sources. Our background values appear to reflect such a signature of normal marine conditions.

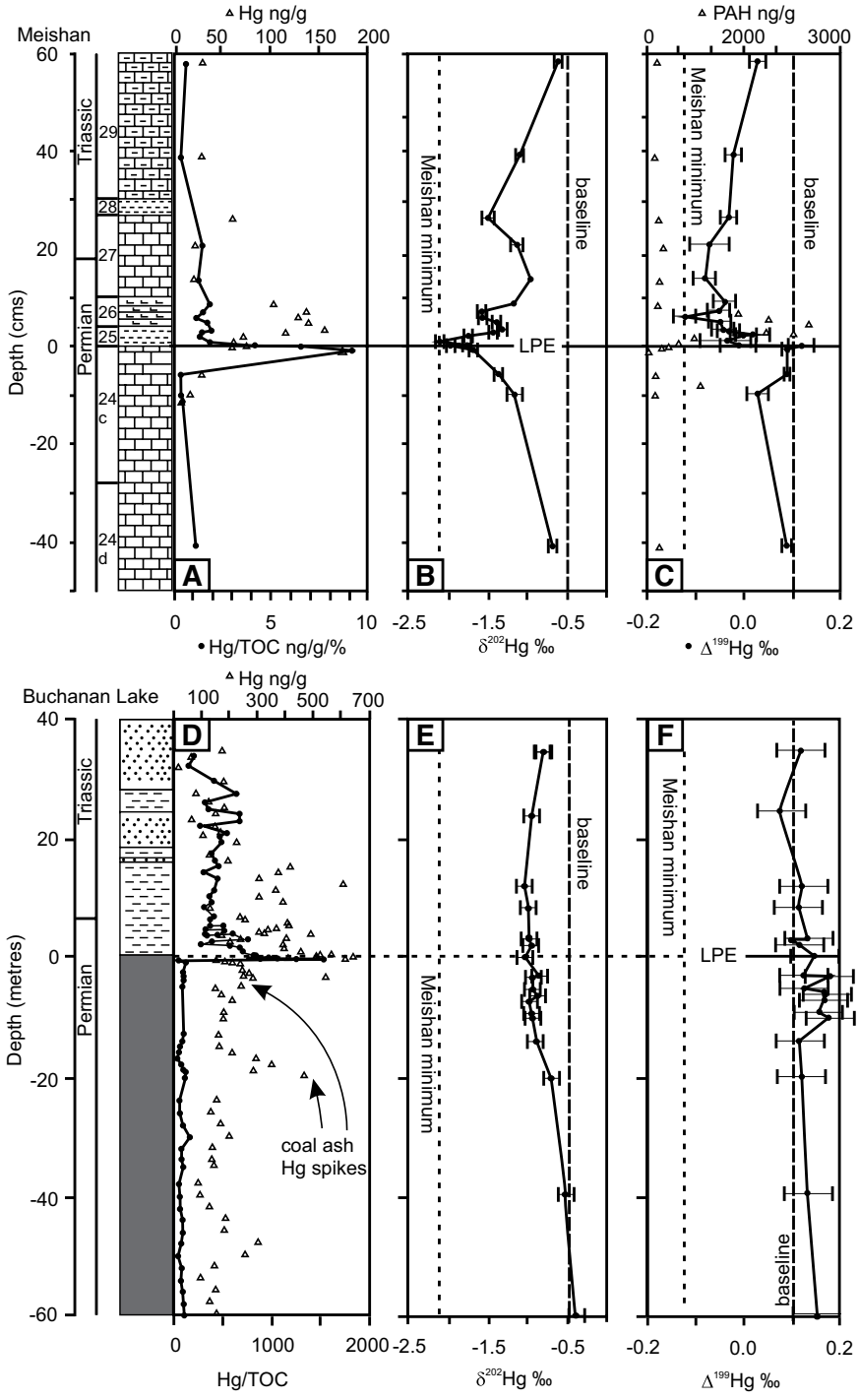

Figure 2. A–F: Geochemical plots for Buchanan Lake (Sverdrup Basin, Canadian Arctic Archipelago) and Meishan (China). Plots show variation of Hg, Hg/TOC (total organic carbon), and stable isotope values for mass-dependent fractionation (MDF; δ^{202}Hg) and mass-independent fractionation (MIF; ^{199}Hg) of Hg deposited in sediment across the latest Permian extinction event (LPE). Vertical dashed lines in both C and F illustrate baseline and minimum values at Meishan to aid comparison. Hg spikes related to coal ash deposition at Buchanan Lake (Sanei et al., 2012; Grasby et al., 2011) are also indicated. PAH—polycyclic aromatic hydrocarbon.

Geogenic Hg sources have insignificant Hg-MIF (Δ^{199}Hg ~0‰) signatures (Smith et al., 2008; Sherman et al., 2009; Yin et al., 2016). However, volcanic plume particles absorb HgII(g) from the atmosphere with positive Δ^{199}Hg (Rolison et al., 2013), providing a plausible explanation for the observed positive Δ^{199}Hg baseline values, particularly at Buchanan Lake. We argue that our background values reflect a dominant input of volcanic-sourced Hg by atmospheric Hg(II) deposition and/or enhanced Hg(II) photoreduction in the water column due to greater

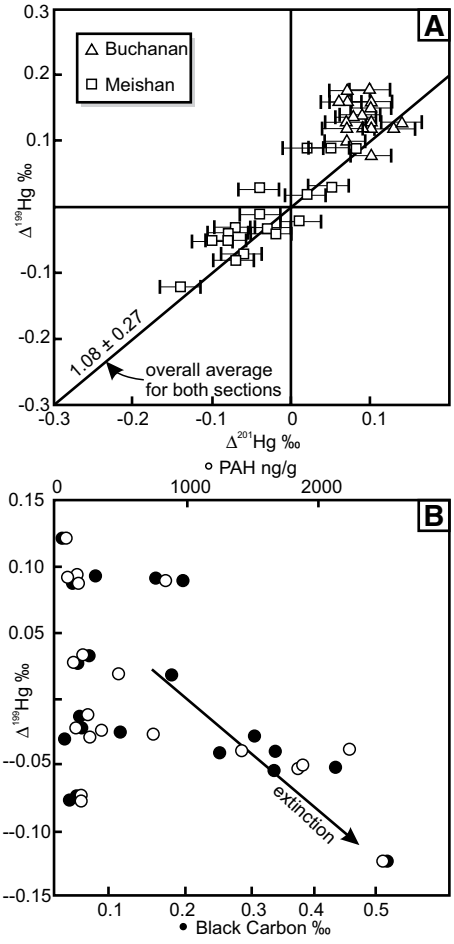

Figure 3. Cross plots of geochemical data from sites examined here. A: Plot showing mass-independent fractionation (MIF) signatures consistent with photoreduction of aqueous Hg(II). B: Cross plot of Δ^{199}Hg data vs. black carbon and polycyclic aromatic hydrocarbon (PAH) data from the Meishan section (China), as measured on the same samples and reported in Shen et al. (2011). Errors for Δ^{199}Hg data are equivalent to symbol height in all plots.

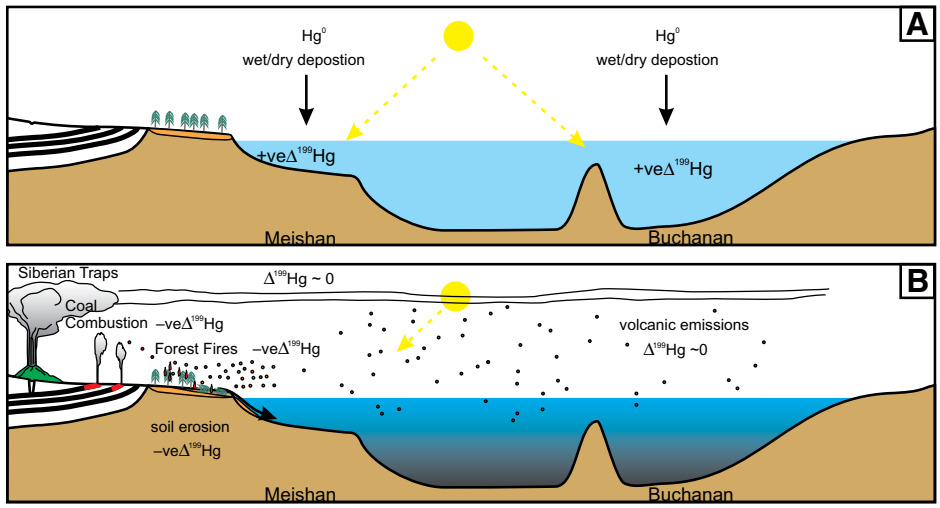

Figure 4. Schematic diagram illustrating conceptual Hg flux to marine environment in Late Permian time, illustrating pre-extinction background conditions (A), and impact of global Hg emissions from volcanic inputs (B) along with additional preferential Hg loading in nearshore environments related to plant combustion and soil erosion sources. Negative (–ve) and positive (+ve) Δ^{199}Hg source signatures are indicated.

water clarity. This is supported by the clastic-starved setting of Meishan, and the deep-water, far-shore setting of Buchanan Lake.

Source of Hg Spikes

During the LPE event, Hg emissions came from volcanic eruptions, as well as burning coal and biomass (Grasby et al., 2015a; Sanei et al., 2012). Active modern volcanic emissions (Zambardi et al., 2009) have δ^{202}Hg = –1.74‰ ± 0.36‰ for gaseous elemental Hg (Hg^0_g) and δ^{202}Hg = –0.11‰ ± 0.18‰ for particulate Hg (Hg^{2+}_p). Terrestrial vegetation accumulates Hg via absorption of wet/dry atmospheric Hg deposition and/or through incorporation of (Hg^0_g) by stomata of leaves (Demers et al., 2013; Yin et al., 2013). Mercury can undergo mass-dependent fractionation during plant uptake of atmospheric Hg, resulting in foliage δ^{202}Hg values ranging from –2‰ to –4‰ (Carignan et al., 2009; Demers et al., 2013; Yin et al., 2013). Modern soils that mainly receive Hg from atmospheric deposition and litterfall have δ^{202}Hg values of –2.0‰ ± 0.6‰ (Demers et al., 2013; Jiskra et al., 2015; Zhang et al., 2013). Given this, all of these potential Hg sources could contribute to the negative δ^{202}Hg shift observed, but they do not have unique δ^{202}Hg signatures such that they can be distinguished.

Volcanoes, the dominant source of Hg, contribute both gaseous Hg(g) and particulate Hg(p) to the atmosphere with no Hg-MIF (Δ^{199}Hg ~ 0‰). At the LPE, the negligible Δ^{199}Hg shift from the deep-marine section at Buchanan Lake (Fig. 2C) suggests that the Hg spike does not relate to a change in the background Hg source (volcanoes). The overall slight positive Δ^{199}Hg values in the sediment likely reflect HgII(g) absorbed from the atmosphere by volcanic ash with positive Δ^{199}Hg values (Rolison et al., 2013). For the coal ash layer below the LPE (Grasby et al., 2011), the Δ^{199}Hg values suggest that the Hg spike represents the early onset of volcanic activity, as in Burgess and Bowring (2015), rather than coal combustion itself. This finding is consistent with Thibodeau et al. (2016), who suggested that stable values of Δ^{199}Hg reflected a dominant volcanic source for an Hg spike at the end-Triassic extinction. In contrast, the negative shift in Δ^{199}Hg values at Meishan is more indicative of increased Hg contribution from biomass and soil sources at the LPE. This is consistent with the observed shift in δ^{202}Hg at Meishan being more negative than Buchanan Lake, as terrestrial organics have significantly lower δ^{202}Hg values than volcanic emissions. The negative shift in Δ^{199}Hg also correlates with previously reported increases in polycyclic aromatic hydrocarbons (PAHs) and abundance of black carbon particles, including char, at the LPE in Meishan (Fig. 3B), which were related to ash deposition from massive wildfires (Shen et al., 2011). Wildfires at this site would not only enhance Hg influx from biomass burning (Pirrone et al., 2010), but might also have promoted soil erosion as a result of significant denudation of vegetation, and the Hg from these sources overwhelmed any signature from enhanced volcanic emissions from the Siberian Traps.

Implications

Stable isotope data suggest that Hg spikes at the LPE came from two prominent sources: (1) volcanic and (2) terrestrial (soil and/or biomass combustion) emissions (Fig. 4). The MIF signatures from Buchanan Lake record enhanced background volcanic Hg loading and, given its distal deep-water and downwind setting (Grasby et al., 2011), provide direct evidence for widespread volcanic impacts on the global environment. However, stable isotope records from the nearshore, shallower-water setting of Meishan show that this background volcanic signal was overwhelmed by Hg from a terrestrial source. This implies that shallow-marine environments had an even larger Hg flux related to massive soil erosion and/or biomass combustion. This is critical because nearshore shallow-water environments are key areas of primary productivity related to upwelling of nutrient-rich waters along continental margins (Chavez and Messié, 2009). While increased background emissions from volcanic sources at the LPE could have stressed global ecosystems (Sanei et al., 2012), especially high levels of Hg input into shallow-water marine environments could have been particularly severe.

CONCLUSIONS

Hg stable isotope data show that prior to the LPE, deep- to shallow-water marine records have similar background δ^{202}Hg values that represent original geogenic sources. At the LPE, a Hg spike, global in extent, is observed. Stable isotope data from distal deep-water locations suggest volcanic emissions had widespread Hg loading impacts on the global environment. In contrast, nearshore, shallower-water settings appear to have received additional Hg loading related to massive soil erosion and/or biomass burning. This may have placed additional ecological stress on these shallow-water environments, which were key areas of marine primary productivity.

ACKNOWLEDGMENTS

We acknowledge the U.S. Geological Survey Wisconsin Mercury Research Laboratory and Wisconsin State Laboratory of Hygiene for the use of their laboratory space for the determination of THg concentrations and stable Hg isotopes. Hua Zhang from the Nanjing Institute of Geology and Palaeontology, Chinese Academy of Sciences, helped with collecting the Meishan samples. Marcus Johnson is thanked for his assistance with Hg isotopic analyses at University of Michigan. J. Gleason and J. Blum acknowledge support for this work from National Science Foundation grant OPP-0909264. This is Earth Science Sector, Natural Recourses Canada contribution 20160079.

REFERENCES CITED

Algeo, T.J., and Twitchett, R.J., 2010, Anomalous Early Triassic sediment fluxes due to elevated weathering rates and their biological consequences: Geology, v. 38, p. 1023–1026, doi:10.1130/G31203.1.

Benton, M.J., and Newell, A.J., 2014, Impacts of global warming on Permo-Triassic terrestrial ecosystems: Gondwana Research, v. 25, p. 1308–1337, doi:10.1016/j.gr.2012.12.010.

Bergquist, B.A., and Blum, J.D., 2007, Mass-dependent and -independent fractionation of Hg isotopes by photoreduction in aquatic systems: Science, v. 318, p. 417–420, doi:10.1126/science.1148050.

Blum, J.D., Sherman, L.S., and Johnson, M.W., 2014, Mercury isotopes in earth and environmental sciences: Annual Review of Earth and Planetary Sciences, v. 42, p. 249–269, doi:10.1146/annurev-earth-050212-124107.

Burgess, S.D., and Bowring, S.A., 2015, High-precision geochronology confirms voluminous magmatism before, during, and after Earth's most severe extinction: Science Advances, v. 1, p. e1500470, doi:10.1126/sciadv.1500470.

Carignan, J., Estrade, N., Sonke, J.E., and Donard, O.F.X., 2009, Odd isotope deficits in atmospheric Hg measured in lichens: Environmental Science & Technology, v. 43, p. 5660–5664, doi:10.1021/es900578v.

Chavez, F.P., and Messié, M., 2009, A comparison of eastern boundary upwelling ecosystems: Progress in Oceanography, v. 83, p. 80–96, doi:10.1016/j.pocean.2009.07.032.

Chen, Z.-Q., and Benton, M.J., 2012, The timing and pattern of biotic recovery following the end-Permian mass extinction: Nature Geoscience, v. 5, p. 375–383, doi:10.1038/ngeo1475.

Demers, J.D., Blum, J.D., and Zak, D.R., 2013, Mercury isotopes in a forested ecosystem: Implications for air-surface exchange dynamics and the global mercury cycle: Global Biogeochemical Cycles, v. 27, p. 222–238, doi:10.1002/gbc.20021.

Erwin, D.H., Bowring, S.A., and Yugan, J., 2002, End-Permian mass extinctions: A review, *in* Koeberl, C., and MacLeod, K.G., eds., Catastrophic Events and Mass Extinctions: Impacts and Beyond: Geological Society of America Special Paper 356, p. 363–383, doi:10.1130/0-8137-2356-6.363.

Gehrke, G.E., Blum, J.D., and Meyers, P.A., 2009, The geochemical behavior and isotopic composition of Hg in a mid-Pleistocene Western Mediterranean sapropel: Geochimica et Cosmochimica Acta, v. 73, p. 1651–1665, doi:10.1016/j.gca.2008.12.012.

Grasby, S.E., and Beauchamp, B., 2009, Latest Permian to Early Triassic basin-to-shelf anoxia in the Sverdrup Basin, Arctic Canada: Chemical Geology, v. 264, p. 232–246, doi:10.1016/j.chemgeo.2009.03.009.

Grasby, S.E., Sanei, H., and Beauchamp, B., 2011, Catastrophic dispersion of coal fly ash into oceans during the latest Permian extinction: Nature Geoscience, v. 4, p. 104–107, doi:10.1038/ngeo1069.

Grasby, S.E., Sanei, H., Beauchamp, B., and Chen, Z., 2013, Mercury deposition through the Permo-Triassic biotic crisis: Chemical Geology, v. 351, p. 209–216, doi:10.1016/j.chemgeo.2013.05.022.

Grasby, S.E., Beauchamp, B., Bond, D.P.G., Wignall, P., Talavera, C., Galloway, J.M., Piepjohn, K., Reinhardt, L., and Blomeier, D., 2015a, Progressive environmental deterioration in northwestern Pangea leading to the latest Permian extinction: Geological Society of America Bulletin, v. 127, p. 1331–1347, doi:10.1130/B31197.1.

Grasby, S.E., Beauchamp, B., Bond, D.P.G., Wignall, P.B., and Sanei, H., 2015b, Mercury anomalies associated with three extinction events (Capitanian crisis, latest Permian extinction and the Smithian/Spathian extinction) in NW Pangea: Geological Magazine, v. 153, p. 285–297, doi:10.1017/S0016756815000436.

Jiskra, M., Wiederhold, J.G., Skyllberg, U., Kronberg, R.-M., Hajdas, I., and Kretzschmar, R., 2015, Mercury deposition and re-emission pathways in boreal forest soils investigated with Hg isotope signatures: Environmental Science & Technology, v. 49, p. 7188–7196, doi:10.1021/acs.est.5b00742.

Pacyna, J.M., and Pacyna, E.G., 2001, An assessment of global and regional emissions of trace metals to the atmosphere from anthropogenic sources worldwide: Environmental Reviews, v. 9, p. 269–298, doi:10.1139/a01-012.

Percival, L.M.E., Witt, M.L.I., Mather, T.A., Hermoso, M., Jenkyns, H.C., Hesselbo, S.P., Al-Suwaidi, A.H., Storm, M.S., Xu, W., and Ruhl, M., 2015, Globally enhanced mercury deposition during the end-Pliensbachian extinction and Toarcian OAE: A link to the Karoo-Ferrar large igneous province: Earth and Planetary Science Letters, v. 428, p. 267–280, doi:10.1016/j.epsl.2015.06.064.

Pirrone, N., et al., 2010, Global mercury emissions to the atmosphere from anthropogenic and natural sources: Atmospheric Chemistry and Physics Discussion, v. 10, p. 4719–4752, doi:10.5194/acpd-10-4719-2010.

Rolison, J.M., Landing, W.M., Luke, W., Cohen, M., and Salters, V.J.M., 2013, Isotopic composition of species-specific atmospheric Hg in a coastal environment: Chemical Geology, v. 336, p. 37–49, doi:10.1016/j.chemgeo.2012.10.007.

Sanei, H., Grasby, S.E., and Beauchamp, B., 2012, Latest Permian mercury anomalies: Geology, v. 40, p. 63–66, doi:10.1130/G32596.1.

Shen, W., Lin, Y., Xu, L., Li, J., Wu, Y., and Sun, Y., 2007, Pyrite framboids in the Permian-Triassic boundary section at Meishan, China: Evidence for dysoxic deposition: Palaeogeography, Palaeoclimatology, Palaeoecology, v. 253, p. 323–331, doi:10.1016/j.palaeo.2007.06.005.

Shen, W., Sun, Y., Lin, Y., Liu, D., and Chai, P., 2011, Evidence for wildfire in the Meishan section and implications for Permian-Triassic events: Geochimica et Cosmochimica Acta, v. 75, p. 1992–2006, doi:10.1016/j.gca.2011.01.027.

Sherman, L.S., Blum, J.D., Nordstrom, D.K., McCleskey, R.B., Barkay, T., and Vetriani, C., 2009, Mercury isotopic composition of hydrothermal systems in the Yellowstone Plateau volcanic field and Guaymas Basin sea-floor rift: Earth and Planetary Science Letters, v. 279, no. 1–2, p. 86–96, doi:10.1016/j.epsl.2008.12.032.

Sial, A.N., Lacerda, L.D., Ferreira, V.P., Frei, R., Marquillas, R.A., Barbosa, J.A., Gaucher, C., Windmöller, C.C., and Pereira, N.S., 2013, Mercury as a proxy for volcanic activity during extreme environmental turnover: The Cretaceous-Paleogene transition: Palaeogeography, Palaeoclimatology, Palaeoecology, v. 387, p. 153–164, doi:10.1016/j.palaeo.2013.07.019.

Smith, C.N., Kesler, S.E., Blum, J.D., and Rytuba, J.J., 2008, Isotope geochemistry of mercury in source rocks, mineral deposits and spring deposits of the California Coast Ranges, USA: Earth and Planetary Science Letters, v. 269, p. 399–407, doi:10.1016/j.epsl.2008.02.029.

Thibodeau, A.M., Ritterbush, K., Yager, J.A., West, A.J., Ibarra, Y., Bottjer, D.J., Berelson, W.M., Bergquist, B.A., and Corsetti, F.A., 2016, Mercury anomalies and the timing of biotic recovery following the end-Triassic mass extinction: Nature Communications, v. 7, doi:10.1038/ncomms11147.

Yin, H., Zhang, K., Tong, J., Yang, Z., and Wu, S., 2001, The global stratotype section and point (GSSP) of the Permian-Triassic boundary: Episodes, v. 24, p. 102–117.

Yin, R., Feng, X., and Meng, B., 2013, Stable mercury isotope variation in rice plants (*Oryza sativa* L.) from the Wanshan Mercury Mining District, SW China: Environmental Science & Technology, v. 47, p. 2238–2245, doi:10.1021/es304302a.

Yin, R., Feng, X., Hurley, J.P., Krabbenhoft, D.P., Lepak, R.F., Hu, R., Zhang, Q., Li, Z., and Bi, X., 2016, Mercury isotopes as proxies to identify sources and environmental impacts of mercury in sphalerites: Scientific Reports, v. 6, p. 18686, doi:10.1038/srep18686.

Zambardi, T., Sonke, J.E., Toutain, J.P., Sortino, F., and Shinohara, H., 2009, Mercury emissions and stable isotopic compositions at Vulcano Island (Italy): Earth and Planetary Science Letters, v. 277, p. 236–243, doi:10.1016/j.epsl.2008.10.023.

Zhang, H., Yin, R.-S., Feng, X.-B., Sommar, J., Anderson, C.W.N., Sapkota, A., Fu, X.-W., and Larssen, T., 2013, Atmospheric mercury inputs in montane soils increase with elevation: Evidence from mercury isotope signatures: Scientific Reports, v. 3, p. 3322.

Manuscript received 15 August 2016
Revised manuscript -received 13 October 2016
Manuscript accepted 14 October 2016

Printed in USA